different designs at 1.55 GHz are given below:

| Series Feedback | | | | Conventional | | | |
|---|---|---|---|---|---|---|---|
| NF | $\|S_{11}\|$ | $\|S_{21}\|$ | $\|S_{22}\|$ | NF | $\|S_{11}\|$ | $\|S_{21}\|$ | $\|S_{22}\|$ |
| 0.6 | 22 | 14 | 15 | 0.25 | 5 | 16 | 23 |

In conclusion, the design method of assigning multiple electrical functions to an individual or small group of discrete components has been demonstrated to form an effective miniaturization technique. It has enabled the realization of miniaturized L-band MIC LNA stages to excellent electrical performance. The miniaturization technique is applied both to a conventional design topology as well as to a series feedback configuration. Each LNA is realized on the same size of surface area of 4.8 mm × 8.8 mm. This size is believed to be the most compact L-band MIC LNA reported to date with the optimum noise figure characteristics.


**REFERENCES**

1. R. E. Lehmann and D. D. Heston, "X-Band Monolithic Series Feedback LNA," *IEEE Trans. Microwave Theory Tech.*, Vol. MTT-33, No. 12, Dec. 1985, pp. 1560–1566.



*Received 11-28-94*

Microwave and Optical Technology Letters, 9/1, 29–32



CCC 0895-2477/95


# SIMPLIFIED CLOSED-FORM EXPRESSIONS FOR COMPUTING THE GENERALIZED FRESNEL INTEGRAL AND THEIR APPLICATION TO VERTEX DIFFRACTION


**F. Capolino and S. Maci**
Department of Electronic Engineering
University of Florence
Via Santa Marta 3
50139 Florence, Italy



**KEY TERMS**

*High frequency, diffraction*



**ABSTRACT**

*The generalized Fresnel integral serves as a canonical function for the uniform ray field representation of several high-frequency diffraction mechanisms. In this article, an example of application of this canonical function is examined, which is concerned with the diffraction at a plane angular sector with soft boundary conditions on its faces. Closed-form expressions for computing this canonical function are presented, and it is shown that the approximate formulation adopted herein is accurate and very fast to calculate. © 1995 John Wiley & Sons, Inc.*


## 1. INTRODUCTION

As is well known, in the vicinity of a shadow boundary, the electromagnetic field diffracted by an edge may be described in terms of the Fresnel integral. In this region, the scattered field does not have a ray optical behavior; therefore, its subsequent diffraction mechanisms cannot be treated by a direct application of the uniform theory of diffraction (UTD). The analytical description of the composite shadow boundary transition phenomena involves the generalized Fresnel integral (GFI). This integral was first introduced by Clemmow and Senior [1], and its properties were exhaustively analyzed by Jones [2]. Several authors employed the GFI in double and multiple knife-edge problems [3–5], and, more recently, in vertex diffraction problems [6–8].

In this article, in order to examine practical features of the GFI, the formulation of a vertex diffraction problem is explicitly considered, which is concerned with the diffraction at a plane angular sector interconnecting two straight edges. This formulation is based on that obtained in [9] for the case of an incident plane wave and observation in the far-field zone. Here, an observation point at finite distance from the tip is considered for the case where soft boundary conditions (bc) are imposed on the faces of the plane angular sector. The analytical details of the present formulation are beyond the purpose of this article and may be found in [10]. Here, only the final, high-frequency expression is given as an application of GFI. In particular, the properties of the generalized transition function that describe the vertex first-order transition regions are discussed in connection with the properties of the GFI.

The use of the GFI in the vertex problem, as well as in other diffraction problems, becomes very practical for engineering applications, if accurate, closed-form expressions are available for the GFI. In fact, the direct numerical calculation of this integral is not a straightforward matter, due to rapid oscillations of the integrand that occur for certain combinations of the two real arguments. Although simple approximations have been presented in the literature [1, 11], their range of applicability has not been well specified. For this reason, the regions of applicability of the above approximate existing formulas are investigated and specified. Furthermore, simple closed-form approximations are derived for the remaining regions. Thus, a very efficient, closed-form formulation is obtained to cover the entire argument plane.

## 2. DIFFRACTION AT A SOFT PLANE ANGULAR SECTOR

Let us consider a plane angular sector formed by two straight, semiinfinite edges, which are interconnected with an angle $\Omega$. Suppose that soft bc are imposed on the two faces. At each edge ($n = 1, 2$) it is useful to define a local coordinate system with its origin at the vertex and the $z_n$ axis along the edge; accordingly, a spherical coordinate system $(r, \beta_n, \phi_n)$ is also defined, where $r$ is the distance from the tip and $\phi_n$ vanishes on the top face. Let us also assume a scalar, unit incident plane wave propagating in a direction $(\beta_n', \phi_n')$.

The leading asymptotic diffracted field from this structure can be obtained by using the UTD diffraction coefficients at the two edges. This approach leads to a field discontinuity when the diffraction point disappears from the tip or abruptly changes its location from one edge to the other. This discontinuity should be compensated by a vertex diffraction contribution. This contribution can be obtained by applying a spectral formulation to the diffraction coefficient derived in [9]. This procedure leads to

$$\psi_v = \frac{e^{-jkr}}{4\pi jkr} \frac{(d_{12} + d_{21})T(\bar{\delta}_1, \delta_1, \bar{\delta}_2, \delta_2, kr)}{(\cos\beta_1' - \cos\beta_1)(\cos\beta_2' - \cos\beta_2)}, \quad (1)$$

where

$$d_{mn} = \sin\frac{\phi_n'}{2}[2\sin\beta_n'\sin\Omega(\cos(\beta_n' - \Omega) - \cos\beta_m)]^{1/2} + \sin\frac{\phi_m}{2}[2\sin\beta_m\sin\Omega(\cos\beta_n' - \cos(\beta_m + \Omega))]^{1/2} + [(\cos(\beta_n' - \Omega) - \cos\beta_m) \times(\cos\beta_m - \cos(\beta_n' + U))]^{1/2}, \quad (2)$$

in which $(-1)^{1/2} = -j$ is assumed for the square roots. The generalized transition function (GTF) $T$ is defined as

$$T(\bar{\delta}_1, \delta_1, \bar{\delta}_2, \delta_2, K) = 4j\pi K\frac{(\bar{\delta}_1^2 + \delta_1^2)\delta_1\delta_2}{(\delta_1\bar{\delta}_2 + \delta_2\bar{\delta}_1)}(G(K^{1/2}\delta_1, K^{1/2}\bar{\delta}_1) + G(K^{1/2}\delta_2, K^{1/2}\bar{\delta}_2)), \quad (3)$$

in which the real arguments are

$$\delta_i = \sqrt{2}\sin\left(\frac{\beta_i' - \beta_i}{2}\right), \quad (4)$$

$$\bar{\delta}_i = \pm\sqrt{2\sin\beta_i\sin\beta_i'}\cos\left(\frac{\phi_i' \pm \phi_i}{2}\right), \quad (5)$$

where the upper (lower) signs apply to $\phi_i' < (>)\ \pi$, and the function $G$ in (3) is the GFI, defined as

$$G(x, y) \triangleq \frac{y}{2\pi}e^{jx^2}\int_x^\infty \frac{e^{-jt^2}}{t^2 + y^2}\,dt. \quad (6)$$

The GTF in (3), which was first introduced in [6], reduces to unity for large $K = kr$, namely, at far-field distance from the tip, as usually happens in the standard UTD transition function.

In order to obtain the complete scattered field from the plane angular sector, both the geometrical-optics (GO) field and the first-order UTD diffracted field from the two edges should be added to the vertex diffracted field in (1). Furthermore, it is worth noting that the double diffraction contribution for this soft case is of a higher asymptotic order and can be neglected in the present analysis.

When the observation point crosses the cone defined by $\beta_i = \beta_i'$ (shadow boundary cone, SBC), the first-order diffraction point on the $i$th edge disappears from the tip and a discontinuity occurs in the dominant asymptotic contribution. It is worth noting that the diffracted field in (1) exhibits apparent singularities at the SBCs. As can be inferred from (4) and the formulas that are presented in the next section for the GFI, the GTF vanishes at the same SBCs; here the vertex contribution $\psi_v$ in (1) is limited and discontinuous to compensate for the discontinuities of the first-order contributions.

The peculiarity of the GTF is that of changing the spreading factor of the vertex contribution depending on the observation point. Close to a SBC, one of the parameters $\delta_i$ vanishes and the GTF provides a cylindrical spreading factor in $\psi_v$ that allows compensation for the discontinuity of the UTD first-order contributions. When the observation point approaches the intersection between the two SBCs, the GO contribution also disappears. In this case, both the parameters $\delta_i$ and $\bar{\delta}_i$ vanish and the GTF produces a plane wave unit spreading factor, which allows compensation for the GO discontinuity also.

In the next section, closed-form expressions for calculating the GFI are presented. These expressions not only allow the GTF properties discussed above to be verified, but also serve as an accurate algorithm for calculating the GTF with an effort that is comparable with that for computing the ordinary UTD transition function.

## 3. CLOSED-FORM EXPRESSIONS FOR THE GFI

In the present case, as in most practical cases in diffraction problems, the arguments $x$ and $y$ of the GFI are real numbers. Taking into account that $G$ is antisymmetric with respect to both the variables, that is [2],

$$G(x, y) = -G(-x, y) = -G(x, -y), \quad (7)$$

we restrict the present analysis to the quarter plane $x \geq 0$, $y \geq 0$. Next, this same region is subdivided in seven regions as shown in Figure 1. Different approximate formulas are employed in each region and the various boundaries are chosen in order to minimize the discontinuity between the relevant contiguous approximations.

All the above approximations involve only the ordinary Fresnel integral defined as

$$F(\xi) = e^{j\xi^2}\int_\xi^\infty e^{-jt^2}\,dt, \quad (8)$$

which can be quickly calculated by employing the simple series expansions given in [12]. For our purpose, the small argument series expansion suggested in this reference has been extended up to $\xi = 12$ by retaining a number of terms equal to $12\sqrt{\xi}$. Furthermore, 11 terms of the asymptotic expansion have been retained for $\xi > 12$. In this way, a truncation error less than $5 \times 10^{-6}$ has been found for all the values of $\xi$.

For the sake of convenience, we will adopt the notation $G_i(x, y)$ to denote the approximation of $G(x, y)$ in the $i$th region ($i = 1, 7$).

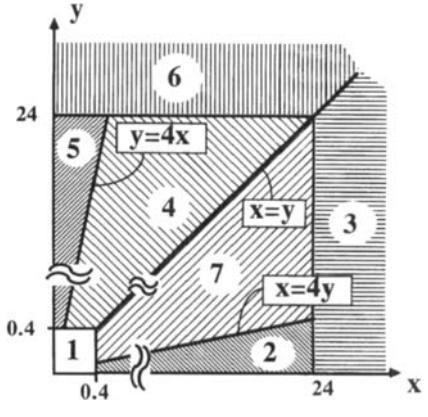


**Figure 1** Subdivision of the argument plane for the various approximations

In region 1 ($x < 0.4$; $y < 0.4$), the GFI has been approximated by using [11]:

$$G_1(x,y) = \frac{1}{2}\exp(jx^2)\left[\frac{1}{\sqrt{\pi}}e^{j(\pi/4)}F(y) - \frac{1}{\pi} \times\left[(1+jy^2)\tan^{-1}\frac{x}{y} - jxy\right]\right], \quad (9)$$

which is easily obtained (a) first by adding to and subtracting from (6) an integral from zero to $x$; thus, the integral from 0 to $\infty$ is easily recognized as a standard Fresnel integral; (b) next a quadratic approximation of the exponential function is used in the remaining integral contribution; (c) finally, this latter approximate expression is integrated by parts.

In region 2 ($0.4 < x < 24$, $x > 4y$), a suitable approximation is obtained by first replacing $(t^2 + y^2)^{-1}$ by its expansion in powers of $(y/t)^2$, and then integrating the first three terms to yield

$$G_2(x,y) = \frac{1}{2\pi}\frac{y}{x}[1 - 2jxF(x)] - \frac{1}{6\pi}\left(\frac{y}{x}\right)^3[1 - 2jx^2 - 4x^3F(x)]. \quad (10)$$

Although the above procedure is the same as that adopted in [1], it is worth noting that our formula does not coincide with Eq. (14) of [1], due to a typographical error in the same reference.

In region 3 ($x > 24$; $x > y$), the asymptotic approximation [1]

$$G_3(x,y) = \frac{1}{2\pi}\frac{y}{x^2+y^2}F(x) \quad (11)$$

provides quite accurate results. In region 4 ($y/4 < x < y$; $0.4 < y < 24$), the following exact representation [11]:

$$G(x,y) = G_4(x,y) = \frac{1}{2\pi}e^{jx^2}[je^{-jy^2}F^2(y) + I(x,y)] \quad (12)$$

may be employed, in which

$$I(x,y) = \int_{x/y}^{1}\frac{e^{-j\sigma^2y^2}}{\sigma^2+1}d\sigma. \quad (13)$$

In this region, the above integral can be calculated without relevant efforts except for high values of $y$ ($y \simeq 20$–$24$). For such values, the integrand in (12) exhibits a rapid oscillatory behavior and the integration may be critical. In order to overcome this difficulty and to improve the algorithm's efficiency, it is found that an approximate explicit expression for $I(x,y)$ may be obtained in terms of standard Fresnel integrals. To this end, the function $(\sigma^2+1)^{-1}$ is expanded in a Taylor series in a neighborhood of $\sigma = 0.6$. By truncating this series at the fourth power of $\sigma$ and integrating it term by term, the following representation is obtained:

$$I(x,y) \simeq \sum_{m=0}^{4} a_m I_m(x,y), \quad (14a)$$

$$a_0 = 0.98926061, \quad (14b)$$

$$a_1 = 0.12808114, \quad (14c)$$

$$a_2 = -1.59843183, \quad (14d)$$

$$a_3 = 1.35987246, \quad (14e)$$

$$a_4 = -0.37895149, \quad (14f)$$

$$I_0(x,y) = \frac{1}{y}[F(x)e^{-jx^2} - F(y)e^{-jy^2}], \quad (15a)$$

$$I_1(x,y) = \frac{j}{2y^2}[-e^{-jx^2} + e^{-jy^2}], \quad (15b)$$

$$I_2(x,y) = \frac{j}{2y^2}\left[-\frac{x}{y}e^{-jx^2} + e^{-jy^2} - I_0(x,y)\right], \quad (15c)$$

$$I_3(x,y) = \frac{j}{2y^2}\left[-\left(\frac{x}{y}\right)^2e^{-jx^2} + e^{-jy^2} - 2I_1(x,y)\right], \quad (15d)$$

$$I_4(x,y) = \frac{j}{2y^2}\left[-\left(\frac{x}{y}\right)^3e^{-jx^2} + e^{-jy^2} - 3I_2(x,y)\right], \quad (15e)$$

which has been found to be very effective.

Finally, in the remaining part of the quarter plane $x > 0$, $y > 0$, the GFI can be calculated by invoking the symmetry property [2, Eq. (A11)]

$$G_n(x,y) = \frac{j}{\pi}F(x)F(y) - G_{n-3}(y,x), \qquad n = 5,6,7. \quad (16)$$

It should be stressed that, although the approximations in (9)–(12) are known in the literature, the regions of their applicability in the argument plane are not well defined by the various authors. Then, our choice of these regions should be carefully checked, particularly across the boundary between contiguous regions, where small discontinuities of $G(x,y)$ may occur. To this end, we have referred to the percent error,

$$\epsilon_{mn}\% = 100 \times |1 - G_m(x,y)/G_n(x,y)|, \quad (17)$$

at the boundary between the adjacent regions $m$ and $n$. Table 1 shows the maximum value of $\epsilon_{mn}$ at every boundary. The worst case occurs at the boundary between regions 1 and 7 ($\epsilon_{17} = 0.65\%$).

Region 4 is covered by the new approximation (12) that has been checked by comparison with a direct, accurate numerical integration. Figure 2 shows the percent amplitude error for $G_4$ in (12) on the four paths shown in the inset of

**TABLE 1 Discontinuities at the Boundaries between Contiguous Approximations**

| $m-n$ | Max $\epsilon_{mn}$ | $m-n$ | Max $\epsilon_{mn}$ | $m-n$ | Max $\epsilon_{mn}$ | $m-n$ | Max $\epsilon_{mn}$ |
|---|---|---|---|---|---|---|---|
| 1 – 5 | 0.02% | 1 – 2 | 0.05% | 7 – 2 | 0.45% | 7 – 3 | 0.24% |
| 1 – 4 | 0.35% | 5 – 4 | 0.03% | 5 – 6 | 0.02% | 2 – 3 | 0.41% |
| 1 – 7 | 0.65% | 4 – 7 | $10^{-4}$% | 4 – 6 | 0.12% | 6 – 3 | 0.18% |

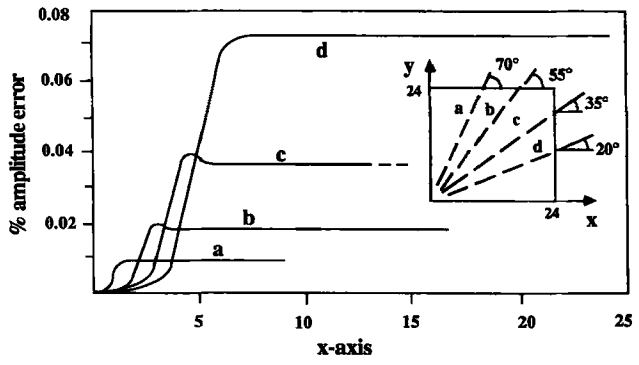


**Figure 2** Percent amplitude error for $G_4$ in Eq. (12), when it is calculated by numerical integration of (13) or by the approximate expression (14)

the same figure. Actually, the relative percent amplitude error exhibits a small oscillatory behavior, and the maximum envelope of each error is plotted in Figure 2. The approximate expressions agree very well with the numerical integration, and a maximum error of 0.07% has been found.

Finally, Figure 3 shows the amplitude and phase level lines of $G(x, y)$ that have been plotted by means of our algorithm. The region $0 < x < 4$, $0 < y < 8$ with a zoom for the region $0 < x < 1$, $0 < y < 1$ has been reported.

## 4. NUMERICAL EXAMPLES

The following numerical examples are devoted to demonstrate both the effectiveness of the formulation (1) in the transition regions close to the SBCs and the accuracy of the GFI calculation by using the approximated formulas presented in the previous section. In Figure 4 and 5, the dashed, dotted, and continuous lines represent the first-order UTD plus the GO fields, the vertex contribution, and the total scattered field, respectively. Figure 4 shows the amplitude (a) and the phase (b) of the scattered field at a distance $r = 2\lambda$ from the tip of an $\Omega = 90°$ plane angular sector. The scan plane and the direction of the incident plane wave are specified in the inset of the same figure, where the SBCs are also depicted. As can be inferred from this figure, when the observation point $P$ passes through these cones, the UTD diffracted field abruptly disappears and the tip contribution provides the required continuity of the total scattered field for both the amplitude and the phase.

The results presented in Figures 5(a) and 5(b) show the scattered field at a distance $2\lambda$, for a plane angular sector with $\Omega = 135°$. The scan plane is symmetrical with respect to the plane angular sector, and the observation point passes through the intersection between two SBCs; in this case, both the GO contribution and the first-order diffracted field contributions simultaneously disappear. As mentioned in Section 2, in this condition all the parameters $\delta_i$ and $\bar{\delta}_i$ in the GFI vanish; again, the tip contribution provides the expected continuity of the total field.

## 5. CONCLUSIONS

At high frequency, the transition regions of multiple diffraction mechanisms are uniformly described by means of generalized transition functions involving the GFI. A diffraction problem in which the GFI plays an important role is that of a vertex discontinuity. A high-frequency formulation for the diffracted field at a vertex in a plane angular sector as been

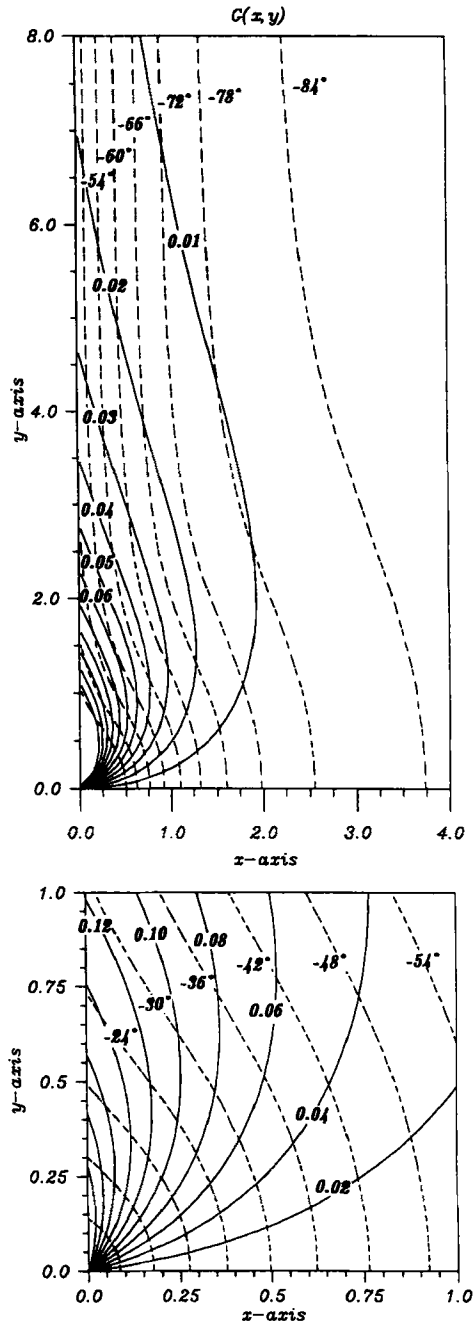


**Figure 3** Amplitude- (solid lines) and phase- (dashed lines) level lines of $G(x, y)$

presented in terms of GFIs. In order to render this formulation useful for practical engineering problems, accurate closed-form formulas for calculating the GFI have been presented. Simple, approximate expressions have been suggested that involve only elementary functions and the ordinary Fresnel integral. In this way, the calculation of generalized transition functions occurring in vertex and multiple diffraction problems is not more complicated than the calculation of the ordinary UTD transition functions of the wedge canonical problem.

The accuracy of the algorithm for the GFI has been demonstrated by testing the relative discontinuity between adjacent approximations and the present error with respect to the direct numerical integration. Furthermore, its applica-

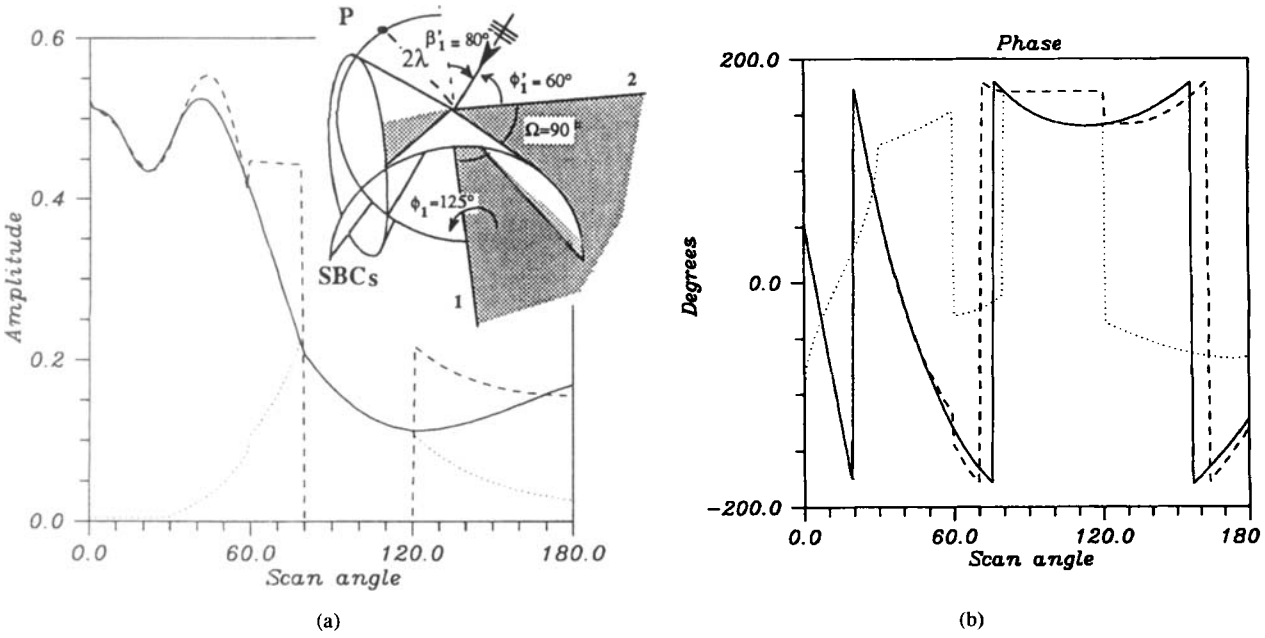


(a) (b)

**Figure 4** Amplitude (a) and phase (b) of the field scattered from a soft plane angular sector. ( $\beta_1' = 80°$, $\phi_1' = 60°$, $\phi_1 = 125°$, $r = 2\lambda$, $\Omega = 90°$. Dashed lines, first-order UTD; dotted lines, vertex contribution; solid lines, total field)

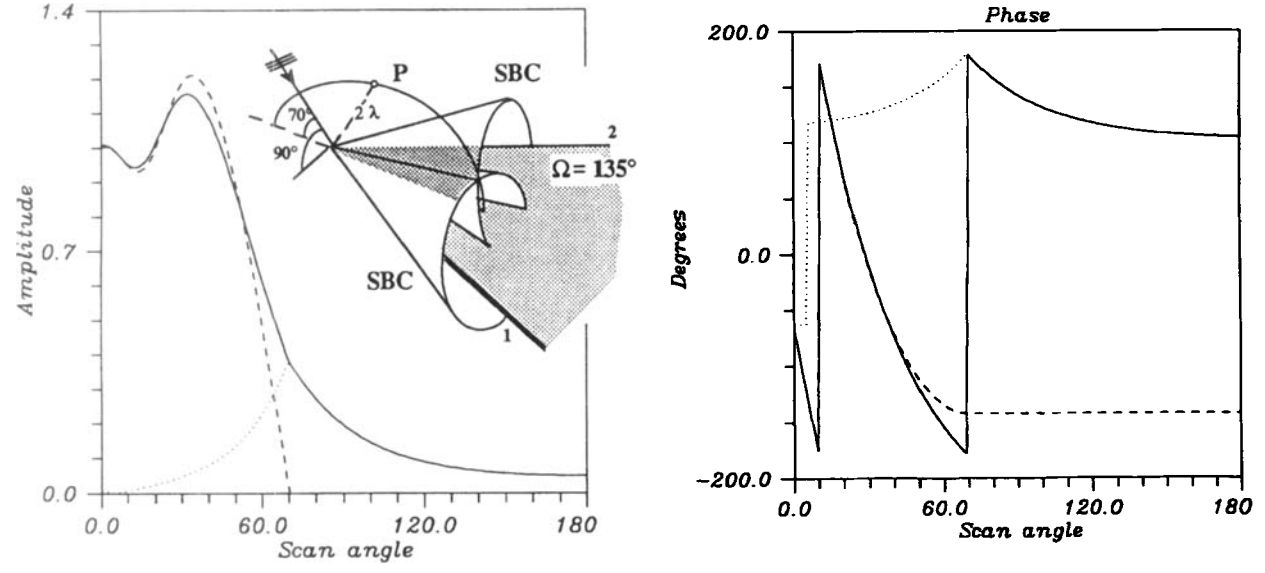


(a) (b)

**Figure 5** Amplitude (a) and phase (b) of the field scattered from a soft plane angular sector. (Scan plane symmetric with respect to the plane angular sector; $r = 2\lambda$, $\Omega = 135°$. Dashed line, first-order UTD + GO; dotted lines, vertex contribution; solid lines, total field)

tion in the vertex problem has shown a good performance in the uniform description of the transition regions.

## REFERENCES


1. P. C. Clemmow and T. B. A. Senior, "A Note on a Generalized Fresnel Integral," *Proc. Cambridge Philos Soc.*, Vol. 49, 1953, pp. 570–572.
2. D. S. Jones, "A Uniform Asymptotic Expansion for a Certain Double Integral," *Proc. R. Soc. Edinburgh Ser. A*, Vol. 69, 1971, pp. 205–226.
3. G. L. James and G. D. Poulton, "Double Knife-Edge Diffraction for Curved Screens, *Microwaves, Opt. Acoust.*, Vol. 3, 1979, pp. 221–123.
4. Y. Ramat-Samii and R. Mittra, "On the Investigation of Diffracted Fields at the Shadow Boundaries of Staggered Parallel Plates, a Spectral Domain Approach," *Radio Sci.*, Vol. 12, 1977, pp. 659–670.
5. L. P. Ivrissimtzis and R. J. Marhefka, "Double Diffraction at a Coplanar Skewed Edge Configuration," *Radio Sci.*, Vol. 26, 1991, pp. 821–830.
6. K. H. Hill, "A UTD Solution to the EM Scattering by the Vertex of a Perfectly Conducting Plane Angular Sector," Ph.D. thesis,

Ohio State University, Department of Electrical Engineering, 1990.
7. L. P. Ivrissimtzis and R. J. Marhefka, "A Note on Double Edge Diffraction for Parallel Wedges," *IEEE Trans. Antennas Propagat.*, Vol. 39, 1991, pp. 1532–1537.
8. L. P. Ivrissimtzis and R. J. Marhefka, "A Uniform Ray Approximation of the Scattering by Polyhedral Structures Including Higher Terms," *IEEE Trans. Antennas Propagat.*, Vol. AP-40, 1992, pp. 1302–1312.
9. S. Maci, R. Tiberio, and A. Toccafondi, "Diffraction at a Plane Angular Sector," *Electromagn. Waves Appl.*, Vol. 8, No. 9/10, 1994, pp. 1247–1276.
10. S. Maci, F. Capolino, and R. Tiberio, "Uniform Diffraction Coefficients at a Plane Angular Sector," *IEEE Trans Antennas Propagat.*, to be published.
11. G. L. James, *Geometrical Theory of Diffraction for Electromagnetic Waves*, Peter Peregrinus, London, 1976, Sect. 2.2, pp. 19–21.
12. E. D. Constantinides and R. J. Marhefka, "Efficient and Accurate Computation of the Incomplete Airy Function," *Radio Sci.*, Vol. 28, 1993, pp. 441–457.

*Received 12-1-94*

Microwave and Optical Technology Letters, 9/1, 32–37

CCC 0895-2477/95

# POLARIZATION BEHAVIOR OF SPUN FIBER VERSUS CONVENTIONAL FIBER UNDER STRONG SLIGHT TWISTING

**Huang Hung-chia**
Shanghai University
Shanghai 201800, China

**He Ying-chun**
Shanghai Institute of Laser Technology
Shanghai 200233, China

**KEY TERMS**

*Fiber optics, polarization optics, optoelectronics, photonics, specialized fiber*

**ABSTRACT**

*In this article, the authors attempt to treat both strong twisting and slight twisting of fiber via a consistent asymptotic approach to the coupled-mode theory. In strong twisting, an admirably simple and useful asymptotic equation is derived in the form $R^2\tau$ = const., which relates the minimum required twist rate $\tau$ with the minimum allowable radius of curvature R. In slight twisting, an oscillatory pattern of the polarization behavior clearly reveals the advantageous feature of a twist-spun fiber, which is made by a prior spinning of the fiber before a twisting. © 1995 John Wiley & Sons, Inc.*

## INTRODUCTION

Around the late 1970s, when the technology of making conventional optical fiber was fairly well established, attempts had begun to make polarization-maintaining fibers in view of the need of a stable mode, or a stable polarization, during transmission. For the past 15 years or more, R & D regarding specialized fibers to maintain linearly polarized light, and to maintain circularly polarized light, ran an almost parallel race. Although linearly polarized light has been used almost exclusively in fiber-optic practice, the advantages of light transmission in circularly polarized light were recognized early by scientists engaged in this art.

Over the past 15 years the advances in R & D regarding specialized optical fibers has turned out to be much more in favor of polarization-maintaining fibers for linearly polarized light. A multitude of linear-polarization-maintaining or hi-bi (highly birefringent) fibers were successfully fabricated around the early 1980s, notably the bow-tie [2], the Panda, and the elliptical-cladding fibers, and have been applied to many practical fiber-optic systems. In contrast, despite the fact that assiduous efforts have been made in devising specialized fiber structures for circular-polarization-maintaining fibers, the advancements made in R & D regarding practical circular-polarization-maintaining fibers have been by far less fruitful [3]. The only means available to produce a practical circular-polarization-maintaining fiber is still to twist a conventional fiber [4].

The circular-polarization-maintaining property of twisted fiber has been extensively studied theoretically and experimentally in the literature [1–3, 5]. Because the twist rate cannot be too large because of the need to maintain mechanical strength, the twist-induced circular birefringence achieved is orders of magnitude lower than the linear birefringence achieved in the said linear-polarization-maintaining fibers. Because of the low circular birefringence induced by way of twisting, it has appeared difficult to employ long lengths of twisted fiber which require curved sections to negotiate a natural course of the transmission line, and are required to resist a variety of random perturbations [6]. For short fiber-optic devices, which can be packaged in a conditioned artificial environment, it remains of interest to explore if it is feasible to use twisted fiber for the transmission of light of a circular SOP (state of polarization).

The aim of this article is to make a relatively comprehensive and in-depth study of the SOP behaviors of twisted fiber in general, and twist-spun fiber in particular, in order to carefully explore the scope of their actually probable utility. Treated in the article are two kinds of problems relating to twisting of fiber.

One problem concerns strong twisting of fiber. Central to the problem is to examine whether or not some kind of fiber strongly twisted within the limit of its mechanical strength can achieve a circular birefringence strong enough to suppress the extrinsic linear birefringence due to a rough bending or an intensive transverse pressure likely to occur in practice.

The other problem concerns slight twisting of fiber, which is laid practically straight. What is of concern in this problem is the occurrence of violent pulsations of the SOP, and how such violent SOP pulsations are related to the intrinsic birefringence of the fiber. The said problems of strong twisting and slight twisting are both dealt with via the coupled-mode analyses.

## ANALYTIC APPROACH VIA COUPLED MODES

For a twist-spun single-mode fiber, the two local modes $W_1$ and $W_2$, which refer to normal modes in the fiber at its unspun state, satisfy the coupled-mode equations:

$$dW_1/dz = -j(\beta - \Delta\beta/2)W_1 + cW_2, \quad (1)$$

$$dW_2/dz = -cW_1 - j(\beta + \Delta\beta)W_2, \quad (2)$$

in which $\beta = (\beta_1 + \beta_2)/2$, $\Delta\beta = (\beta_1 - \beta_2)$, and $c$ is the coupling coefficient. In principle, Eqs. (1) and (2) apply